Journal of Radioanalytical and Nuclear Chemistry
https://doi.org/10.1007/s10967-023-09294-5

Development and applications of accelerator mass spectrometry methods for measurement of ^{14}C, ^{10}Be and ^{26}Al in the CENTA laboratory

Pavel P. Povinec[1] · Ivan Kontuľ[1] · Miroslav Ješkovský[1] · Jakub Kaizer[1] · Jakub Kvasniak[1] · Ján Pánik[2] · Jakub Zeman[1]

Received: 16 September 2023 / Accepted: 24 November 2023

Abstract
Terrestrial and extraterrestrial radioisotope research has been strongly dependent on the development of analytical methods which would enable to trace radioisotopes at low concentrations in subgram samples (e.g., in tree rings, ice cores, meteorites, etc.). Accelerator mass spectrometry (AMS) has become the most sensitive technique for ultralow-level analysis of long-lived radioisotopes, such as ^{14}C, ^{10}Be and ^{26}Al. We review developments and applications carried out in the CENTA laboratory, and describe a recently installed fully equipped AMS line, designed for analysis of long-lived radioisotopes from tritium to curium.

Keywords AMS · Radionuclides · ^{14}C · ^{10}Be · ^{26}Al · CENTA

Introduction

Many scientific investigations from very different fields have been crucially dependent on the sensitivity, accuracy and precision of radioisotope measurements in various types of samples, as well as on the radio-contamination of instruments used for such investigations. A high precision direct measurement of radionuclide activity in very small samples has been a challenging process, requiring a very low instrumental background and high efficiency of radionuclide analysis in small samples [1]. Therefore, many applications have not been possible (in nuclear as well as in environmental sciences) either because of low sensitivity of analysis or due to the requirement of too large samples, which have not been available. Recent radioisotope levels observed in the environment have been very low (especially those of anthropogenic origin from global fallout), therefore, highly sensitive radioanalytical systems have to be constructed for carrying new environmental investigations. Important developments have been reached with large volume Ge detectors operating in deep underground laboratories, where contributions from cosmic rays have been negligible, however, multigram samples have sometimes been required to get comparable limits with mass spectrometry measurements [2, 3]. The main developments in mass spectrometry methods have been due to improvements in inductively coupled plasma mass spectrometry (ICPMS) technologies, where detection limits below 1 nBq/g have been reached even for sample sizes about 1 g [4, 5]. The most sensitive technology for analysis of long-lived radioisotopes has become, however, accelerator mass spectrometry (AMS) due to a considerable decrease in instrumental background (operating the instruments at higher energies), and an efficient isobar removal, therefore ultra-low detection limits have been reached even for mg samples, approaching in some applications single atom counting [6, 7].

These developments have been well demonstrated in environmental and climate change studies using isotope archives, e.g. ^{14}C in tree rings [8], ^{10}Be and ^{36}Cl in ice cores [9, 10], which has also been important for a better understanding of the impact of the Sun on Earth, e.g., via solar activity cycles [11, 12] and solar particle events (observed during large solar eruptions) [13], which could also influence space weather, important for future human missions in cosmic space.

✉ Pavel P. Povinec
pavel.povinec@uniba.sk

[1] Department of Nuclear Physics and Biophysics, Faculty of Mathematics, Physics and Informatics, Centre for Nuclear and Accelerator Technologies (CENTA), Comenius University, 84248 Bratislava, Slovakia

[2] Faculty of Medicine, Institute of Medical Physics, Biophysics, Informatics and Telemedicine, Comenius University, 81372 Bratislava, Slovakia

Published online: 09 January 2024

Environmental research has been especially strongly influenced by cosmogenic radioisotopes, such as ^{14}C and ^{10}Be, due to their relatively high production rates in the stratosphere and troposphere by secondary cosmic-ray particles with oxygen and nitrogen atoms, their transport to ground-level air, to the hydrosphere (including oceans) and biosphere, and then storage in isotope archives with yearly resolution (tree rings, ice cores), and availability of ultrasensitive AMS technology for their analysis in annual samples [9, 10, 14, 15]. Cosmogenic radioisotopes have been widely used in astrophysics, in studies of environmental processes and environmental pollution, in the dating of geological samples, as well as in the dating of historical events and cultural heritage samples.

There has been another group of radioisotopes of anthropogenic origin, produced in the atmosphere during atmospheric tests of nuclear bombs carried out mainly in the 1950s and early 1960s. Maximum ^{14}C levels in the atmosphere peaked in 1963, when in the northern hemisphere they were by 100% above cosmogenic production [16], and similarly in the biosphere a year later [17]. The present ^{14}C levels in the atmosphere and biosphere are, however, almost the same as they were during the pre-bomb era [8].

Many other anthropogenic radionuclides (e.g., ^{3}H, ^{90}Sr, ^{99}Tc, ^{129}I, $^{135,137}Cs$, ^{241}Am, Pu isotopes) were produced in nuclear bomb explosions (global fallout), during Chernobyl and Fukushima accidents, and released from nuclear reprocessing facilities (Sellafield in UK and Le Hague in France), which have been widely used as tracers studying environmental processes and impacts of nuclear industry on the environment [18, 19].

Radioactive isotopes therefore represent unique tracers of environmental processes, allowing to study not only processes of their origin, but also their spread in the atmosphere and in other Earth's reservoirs, up to their final storage in isotope archives that record their temporal evolution (tree rings, glaciers, stalagmites/stalactites, corals, freshwater and marine sediments) [8].

In this paper, we review development of AMS methods for analysis of ^{14}C, ^{10}Be and ^{26}Al in environmental samples, carried out at the CENTA laboratory. Further activities also included the development of methods for the analysis of ^{129}I, and isotopes of Th, U and Pu [20–22]. We describe shortly also the recently installed fully equipped AMS beam line, designed for analysis of long-lived radioisotopes from tritium to curium.

Carbon-14

The radioisotope most commonly used in environmental studies has been ^{14}C due to its suitable half-life (5700 y), availability in environmental archives, and the development of ultrasensitive AMS methods for its analysis. ^{14}C after its production in the atmosphere is oxidized to CO and later to CO_2, which is after stratosphere-troposphere mixing transported to the biosphere. Atmospheric CO_2 is exchanged with surface ocean waters and finally it is deposited as carbonates in the deep ocean, where it forms the main carbon reservoir [23].

The large consumption of fossil fuels from the nineteenth century to the present caused increased concentrations of stable carbon isotopes (^{12}C and ^{13}C) in the atmosphere and biosphere (Suess effect [24]), which influenced relative ^{14}C levels in the environment as well. Therefore, radiocarbon in the environment represents a very complex tracer that has been useful in many investigations.

Although the cosmogenic ^{14}C has been crucial in past climate change studies (including solar activity cycles and solar proton events), the anthropogenic ^{14}C (and the Suess effect) has been important for a better understanding of exchange processes in the environment. Radiocarbon became, therefore, important for better understanding of atmospheric processes, atmosphere–hydrosphere and atmosphere–biosphere mixing, processes in seawater and thermohaline circulation in the world ocean [23, 25].

Our involvement in radiocarbon science started in 1966 with the development of proportional counters and vacuum lines for the preparation of CO_2 as a gas filling. Motivation was in the construction of the first Czechoslovak nuclear power plant (NPP) in Jaslovské Bohunice (about 60 km north–east of Bratislava, Fig. 1) with natural uranium as a fuel, heavy water as a moderator and CO_2 as a cooling gas. Due to the presence of nitrogen tracers in CO_2, it was expected that ^{14}C production will not be negligible and, therefore a ^{14}C monitoring system should be established. Our first ^{14}C data were published in 1967 as a start of the pre-operational monitoring, with CO_2 sampling using NaOH solution in Bratislava and Jaslovské Bohunice [26]. Later, a new low-level proportional counter with a better sensitivity using methane filling was developed [27, 28]. The sampling site moved in 1973 from Jaslovské Bohunice to the newly established monitoring station in the nearby Žlkovce village. Also, the Bratislava site moved in 1976 from the city center to the newly built university campus in Mlynská dolina. In 2015 we also included a new sampling site in Tajná, close to the second NPP built in Mochovce. The atmospheric $^{14}CO_2$ data set from Bratislava and Žlkovce stations (Fig. 2) is a result of radiocarbon analysis of continuous monthly sampling of atmospheric CO_2 in NaOH solution. Bratislava sampling has been continuing to the present, producing the second longest continuing ^{14}C record in Europe (after the University of Heidelberg, Germany [29]), and the third one in the world (after New Zealand [30] and Germany).

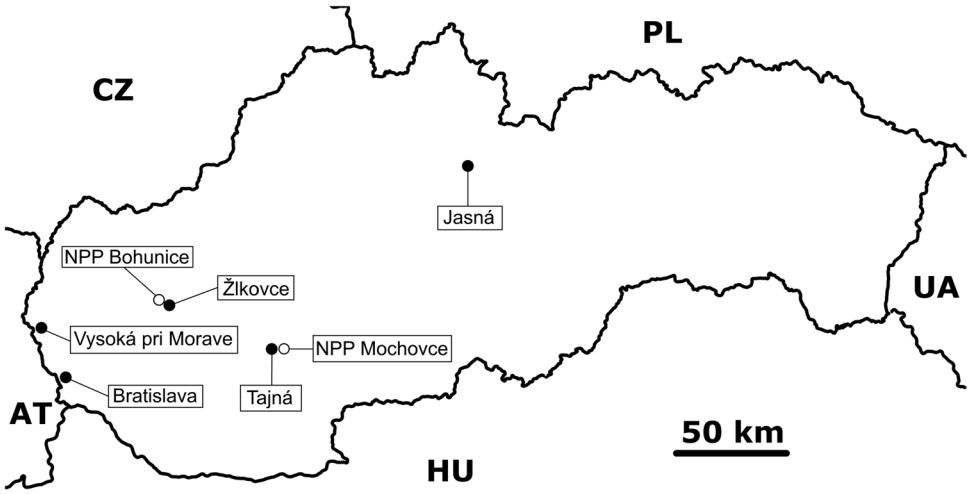

Fig. 1 Map of Slovakia with nuclear power plants (NPP) and atmospheric CO2 and tree-ring sampling stations: (i) Bratislava CO_2 and tree-ring station. (ii) Bohunice NPP built in Jaslovské Bohunice, with monitoring station in Žlkovce. (iii) Mochovce NPP with monitoring station in Tajná. (iv) Sites for an additional tree-ring sampling at Vysoká pri Morave and Jasná (a clean air station) are also shown

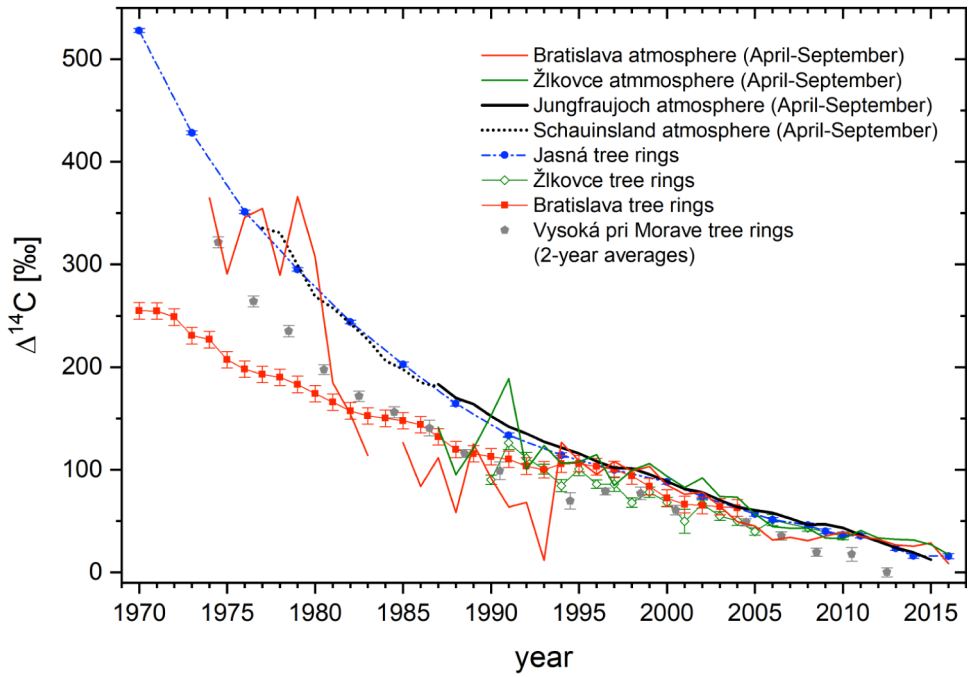

Fig. 2 Comparison of atmospheric $\Delta^{14}C$ data for Bratislava and Žlkovce (monitoring station for the Bohunice NPP) with Slovakia tree-ring data and with Jungfraujoch and Schauinsland clean-air atmospheric data [36]. Atmospheric $\Delta^{14}C$ data include only monthly values for the growing season (April–September)

^{14}C in tree rings

Motivation

Tree rings have been very useful isotopic archives that record annual ^{14}C levels in the biosphere, important for studying transport processes between the atmosphere and the biosphere, for climate change studies and Sun–Earth relations, and for investigating impacts of the nuclear industry on the environment [15, 31]. In 2012 we started with preparation of graphite targets for AMS measurements of ^{14}C in tree ring samples from Žlkovce [31, 32] which were analyzed at cooperating AMS laboratories (VERA laboratory of the University of Vienna, and the Institute for Nuclear Sciences (ATOMKI) in Debrecen). Later, we continued with AMS analyzes of tree ring samples collected in Vysoká pri Morave (25 km north–west of Bratislava), which were used to control ^{14}C levels on the windward side of the Žlkovce and Bratislava stations [33], and in Jasná in central Slovakia, far from any industrial activities, which could represent a clean air station for Slovakia with minimum fossil fuel impacts [34]. We also analyzed ^{14}C in tree rings from a tree cut on the university campus in Mlynská dolina [35].

In this review, we shall compare ^{14}C levels in tree rings from the mentioned localities with the aim of assessing the impact of the Bohunice NPP on the biosphere, and to study the Suess effect in the region. The Žlkovce tree ring record has been specifically used to compare atmospheric

and biospheric ^{14}C levels in Žlkovce village with the objective of assessing the impact of the Bohunice NPP on the environment, while the Bratislava tree ring record has been used to study atmosphere–biosphere relations, influences of fossil fuel combustion in the large city environment, as well as to search for any impacts from the Bohunice NPP on the Bratislava air. The mentioned ^{14}C tree ring data will be compared with the Jasná tree ring data (representing the clean air station for Slovakia), as well as with atmospheric ^{14}C data collected at Jungfraujoch (46.6° N, 8.0° E), 3570 m above sea level, Swiss Alps (data available from 1986) and Schauinsland (47.9° N, 7.9° E), 1205 m above sea level in Black Forest, Bavaria, Germany (ground level data available from 1977), representing European clean air and Germany clean air sites, respectively [36].

Preparation of tree-ring samples

We shall only briefly describe the collected tree ring samples and analytical procedures, as the full description can be found in the cited papers. The Bratislava tree was a black poplar (*Populus nigra*) grown in close proximity to the building of the Faculty of Mathematics, Physics and Informatics of Comenius University in Bratislava, Slovakia (where monthly atmospheric sampling occurs), Fig. 1. The tree section was divided into individual rings that were pretreated with the acid–base-acid method (HCl and NaOH followed by bleaching with $NaClO_2$). The bleached wood samples were then dried and subsequently combusted in a stream of pure oxygen. More details on sample preparation can be found in [35].

Žlkovce tree rings were sampled using an increment borer from a lime tree (*Tilia cordata*) growing near the Žlkovce atmospheric monitoring station (48° 29′ N, 17° 40′ E), Fig. 1 [31]. The sampled core was divided into 21 annual growth rings which were then pretreated using the acid–base-acid method (60 °C 0.5 M HCl, 60 °C 0.5 M NaOH and 60 °C 0.5 M HCl), followed by rinse in distilled water. The dried samples were burned in quartz tubes filled with oxygen and the resulting CO_2 was purified by cold traps and reduced to graphite in a reaction with hydrogen over an iron powder catalyst.

Vysoká pri Morave (48° 19′ N, 16° 54′ E), Fig. 1, tree ring samples were taken from two wooden cores of a Weymouth pine (*Pinus strobus*) [33]. The wood from the center of each ring (to exclude possible contamination by sanding paper) was pretreated and graphite targets were prepared as described for the Žlkovce samples.

Jasná tree-ring samples from a European spruce (*Picea abies*) were collected at the edge of a forest in the vicinity of a recreational area on the northern slope of the Chopok mountain, in the Low Tatras mountain range (48° 58′ N, 19° 34′ E, 1200 m above sea level), Fig. 1, [34]. The sampled core was divided into individual growth rings at the Faculty of Forestry and Wood Technology of Mendel University in Brno (Czech Republic).

Together with analysis of tree ring samples, ^{14}C standard reference materials (SRM-4990C ^{14}C oxalic acid) of the National Institute of Standards and Technology (Gaithersburg, USA), and ^{14}C reference material (IAEA-C3) and background (IAEA-C9) of the International Atomic Energy Agency (IAEA, Vienna, Austria) were used. The activity of ^{14}C acquired by the measurement is reported in terms of age corrected $\Delta^{14}C$ [37]

$$\Delta^{14}C = \left(\frac{A_{SN} \cdot e^{\lambda(y-x)}}{A_{abs}} - 1 \right) \cdot 1000‰$$

where A_{SN} is the normalized activity of the sample, *Aabs* is the activity of the absolute ^{14}C standard, λ is the decay constant of ^{14}C, x is the year of tree ring formation and y is the year of measurement.

Results

A comparison of $\Delta^{14}C$ data on atmospheric $^{14}CO_2$ measurements in Bratislava and Žlkovce, and tree-ring measurements in Bratislava, Žlkovce, Vysoká pri Morave and Jasná, with clean air data from Schauinsland and Jungfraujoch is presented in Fig. 2 (the atmospheric data have been modified for the growing season April–September). The trends observed in the $\Delta^{14}C$ records and deviations from the clean air data (Table 1) show the existence of large differences between the $^{14}CO_2$ and tree ring data measured for Slovakia samples, as well as when compared with clean air stations, especially up to 1995, documenting a strong Suess effect in the south–western Slovakia.

The most complicated situation has been observed for the Bratislava station due to its strong pollution with fossil fuel CO_2 (having zero ^{14}C levels), as a result of heavy industrial activities, especially during the 1980s (up to 1994), when a $\Delta^{14}C$ minimum was observed in 1993 air (close to −200‰). After 1994 the situation has remarkably improved, when the Bratislava data were almost within uncertainties with the Jungfraujoch curve, except for some smaller deviations observed during the middle of 2000s.

This has also been well manifested in the tree-ring data, when up to 1994 a remarkable decrease in Bratislava $\Delta^{14}C$ levels (down to −150‰, Table 2) was observed compared to the Schauinsland clean air data. It is also interesting to mention that the Vysoká pri Morave tree-ring data (representing a country site with only agricultural activities) have always been below the Schauinsland curve (by about 50‰), and in 1994 and 1996 they were even below the Bratislava values.

Similar trends in tree-ring and atmospheric $\Delta^{14}C$ data were also observed in other regions of Central Europe, for

Table 1 Comparison of ^{14}C levels in the atmosphere and tree rings in Slovakia with clean air stations in Schauinsland and Jungfraujoch [36]

Sampling site	Samples	Period	Trend [‰/y]	Deviations from clean air [‰]
Bratislava	$^{14}CO_2$	1973–1994	19.3 ± 2.4	− 115 to + 65
Bratislava	$^{14}CO_2$	1995–2017	4.6 ± 0.4	− 25 to + 15
Žlkovce	$^{14}CO_2$	1987–1994	1.5 ± 5.2	− 75 to + 45
Žlkovce	$^{14}CO_2$	1995–2017	4.6 ± 0.3	− 15 to + 15
Schauinsland[a]	$^{14}CO_2$	1977–1987	16.5 ± 0.9	–
Jungfraujoch[b]	$^{14}CO_2$	1987–1994	8.8 ± 0.4	–
Jungfraujoch[b]	$^{14}CO_2$	1995–2015	5.6 ± 0.1	–
Bratislava	Tree rings	1973–1994	5.8 ± 0.2	− 150 to − 10
Bratislava	Tree rings	1995–2004	5.6 ± 0.5	− 15 to 0
Žlkovce	Tree rings	1990–1994	1.7 ± 5.4	− 50 to − 10
Žlkovce	Tree rings	1995–2005	3.8 ± 0.4	− 5 to 0
Vysoká pri Morave	Tree rings	1974–1994	12.5 ± 1.0	− 70 to − 40
Vysoká pri Morave	Tree rings	1995–2012	4.9 ± 0.3	− 25 to − 10
Jasná	Tree rings	1973–1994	13.4 ± 0.9	–
Jasná	Tree rings	1995–2016	4.6 ± 0.2	–

Table 2 Optimized negative ion beam currents for aluminum species of interest

Material	Ion	Beam current (nA)
Al_2O_3	Al^-	35
	AlO^-	1100
AlN	Al^-	60
	AlO^-	650
	AlN^-	700

example, in Krakow [38–41] and in Prague [42, 43]. The observed trends may have been probably influenced by the recent movement towards constraints on CO_2 emissions.

Žlkovce monitoring station is a very interesting case because it represents an agricultural region influenced by the Suess effect, which could be, however, also influenced by ^{14}C releases from the nearby Bohunice NPP. The atmospheric $\Delta^{14}C$ data confirm these expectations, since elevated levels above the Jungfraujoch curve were observed, e.g., up to 45‰ in 1991, however, the corresponding tree-ring value was below the Jungfraujoch curve by about 20‰. Later, during the 2000s and 2010s, the atmospheric $\Delta^{14}C$ values up to 15‰ were above the Jungfraujoch curve. However, since the Žlkovce site has also been influenced by the regional Suess effect, probably similar to the Vysoká na Morave site, the real Bohunice NPP contribution could be even by about 30‰ higher. A comparison of $\Delta^{14}C$ atmospheric and tree-ring data for the Žlkovce station shows that the ^{14}C tree-ring levels were always below the atmospheric levels by about 50‰, and of course, they were below the Jungfraujoch levels, but even below the Bratislava levels, indicating that short term atmospheric releases due to NPP operation have not been manifested strongly in the tree-ring record. However, the Žlkovce tree-ring data were in some cases higher than the Vysoká pri Morave tree-ring data (up to about 30‰), which could again indicate a possible impact of the NPP on the tree-ring data, although in recent years the differences were smaller.

For a better understanding of ^{14}C in the environment of Slovakia, a clean air station in Jasná (central Slovakia) has been established (Fig. 1). The first important observation is that the Jasná ^{14}C data agrees with the Jungfraujoch and Schauinsland curves, indicating that the Jasná represents well a clean-air station. The differences between the Bratislava and Jasná tree-ring data decreased from about 150‰ down to about 45‰ in 1988, but after 1993 the Bratislava data were within uncertainties comparable with Jasná data.

^{14}C in aerosols

Motivation

Carbonaceous aerosols are an important part of the atmosphere contamination by the particulate matter that has been increasing during the last century due to releases of fossil fuel particles, and recently also due to the growing number of particles of biospheric origin. They have been recognized as important impactors on human health [44], as well as on radiative forcing on Earth [45]. On average, carbonaceous aerosols represent 20–50% of aerosol mass [46], which could be very variable locally and regionally. Carbonaceous aerosols are divided into two fractions: organic carbon (OC,

carbonaceous compounds released from the biosphere or as byproducts of fuel combustion) and elemental carbon (EC, also called black carbon, released into the atmosphere from incomplete combustion of fuels). Especially, the organic carbon fraction, represented by a large number of different organic compounds of primary origin (by-products of combustion) or secondary origin (products of chemical reactions in the atmosphere) requires a specific approach, as demonstrated in many aerosol studies, focused on their sources, formation, and propagation in the atmosphere [47–49]. Radiocarbon analysis of aerosols can distinguish between fossil fuel (zero ^{14}C levels) and biospheric (close to the contemporary ^{14}C levels) origin of aerosols [50]. Although miniature proportional counters could analyze ^{14}C in carbonaceous aerosols with a few mg of carbon as well, the development of AMS technology opened the door to high precision analysis of µg-sized samples [47, 51].

Although we have been studying atmospheric aerosols in Bratislava since 1976 [52, 53], only low-background gamma-spectrometry has been used, which enabled the investigation of gamma-ray emitters, such as ^{7}Be of cosmogenic origin, and many radioisotopes of anthropogenic origin (^{60}Co, $^{134,137}Cs$, ^{241}Am, etc.), as well as of natural origin (primordial ^{40}K, and decay products in ^{232}Th and ^{238}U chains), which were mostly associated with atmospheric contamination studies [54–56], including Chernobyl [52] and Fukushima accidents [56, 57]. Although we did some ^{14}C and ^{137}Cs investigations together [53], ^{137}Cs was on aerosols and ^{14}C was as $^{14}CO_2$. However, with the establishment of the CENTA laboratory, a research on carbonaceous aerosols using AMS technology became feasible.

Sampling of carbonaceous aerosols

The same aerosol sampling system has been used for gamma-emitters and carbonaceous aerosols, using circular quartz microfiber filters (Sartorius T293 0.3 µm, 47 mm in diameter) [57]. The average air flow through the filter was 66 L/min, the sampling period was 14 days, and 800–1500 m^3 of air was pumped through the filter during this period. Filter samples after pretreatment were combusted and the CO_2 obtained was purified to remove sulfur and its compounds, and later it was cryogenically transferred to a graphitization reactor with iron powder catalyst and hydrogen gas. All analytical details can be found in [58].

Results

The ^{14}C analysis of aerosols, used to determine the fractions of EC carbonaceous aerosols produced by fossil fuel combustion and biomass burning (Fig. 3), clearly shows seasonal variations. During the winter months the fossil- and biomass-derived EC aerosol particles had comparable contributions (the average fossil fuel fraction was only 53%), while the biogenic fraction was lower during the rest of the year with minimum in summer, when the contributions of fossil-fuel particles were on average 73% of the total elemental carbon in the air. The contribution of fossil fuel-derived

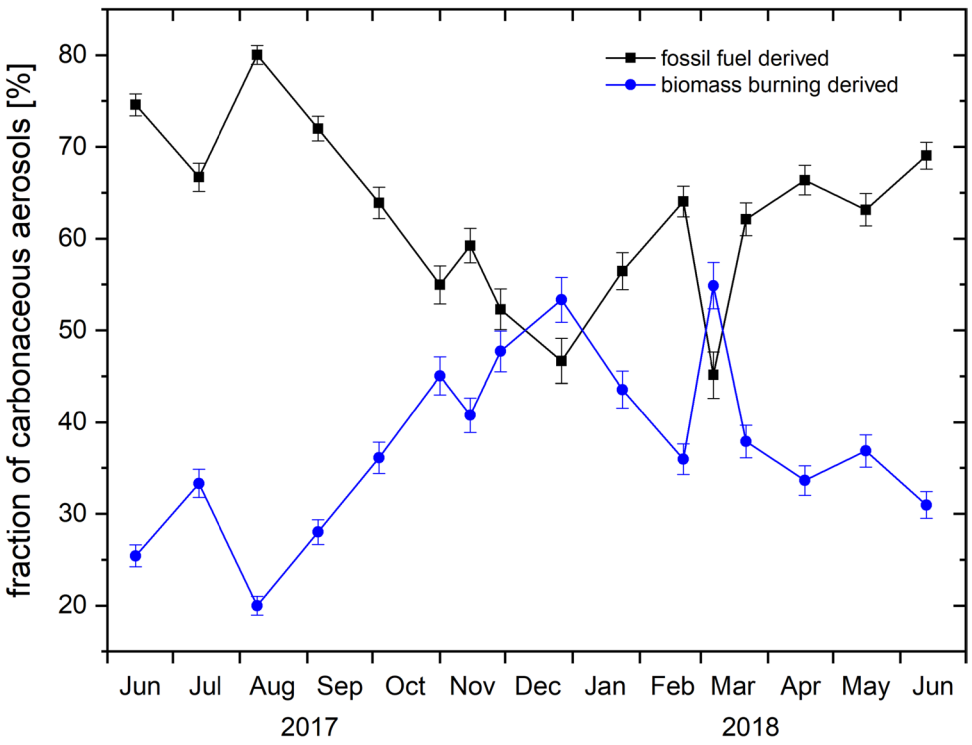

Fig. 3 Fossil-fuel and biomass-burning derived aerosol fractions in Bratislava air

particulate matter decreased then in spring and autumn to 63%. This was due to the fact that, especially at villages due to higher gas prices, a combustion of wood had been very often used for heating. The recently introduced industrial wood combustion used for heating purposes should be contributing as well. Although Bratislava is highly industrialized city, the high proportion of biomass-derived EC aerosol in winter could be caused by domestic wood combustion for heating purposes, particularly in city suburbs and the rural region surrounding Bratislava. The results obtained confirmed that biomass burning may represent potential pollution problems in large cities.

Beryllium-10

Motivation

Cosmogenic ^{10}Be is produced by spallation nuclear reactions induced by cosmic rays in both terrestrial and extraterrestrial materials. In the atmosphere, the main source of ^{10}Be represents its formation by spallation reactions of cosmic-ray particles with oxygen and nitrogen nuclei. ^{10}Be after its production is attached to aerosols and deposited on the Earth surface by wet or dry deposition (meteoric ^{10}Be). The production rate of ^{10}Be in the atmosphere is dependent on the cosmic-ray flux, which is in turn heavily influenced by solar activity and geomagnetic field intensity. Therefore, environmental ^{10}Be records contain retrospective information about solar activity and geomagnetic field, represented for example, by analysis of ^{10}Be in ice cores, which could be directly linked to the changes in solar activity in the past [59]. On the other hand, ^{10}Be measurements of loess sediments make it possible to reconstruct past geomagnetic intensities [60]. Recently, the most exciting ^{10}Be applications were associated with past solar activity and climate changes by analyzing ^{10}Be in ice cores with high time resolution, similarly as it has been done in the case of ^{14}C tree-ring studies [8, 59].

In situ produced ^{10}Be in the lithosphere (e.g., in minerals) can be used in geomorphology studies for surface exposure dating and burial dating. Surface exposure dating is used to determine the age of rocks that were shielded from cosmic rays in larger depths and then were suddenly exposed to cosmic rays by miscellaneous geological processes (glaciers, rivers, landslides, etc.). Measurement of accumulated cosmogenic radionuclides in the sample can lead to the determination of the length of exposure time of the studied formations, for example, glacial moraines or fluvial terraces [61, 62]. Burial dating is used on rocks that have been exposed to cosmic rays and then moved deeper underground or covered with new layers, such as river sediments [63]. The meteoric ^{10}Be measurements include wide applications in geology [64], e.g. in the determination of soil erosion rates [65]. Another interesting application of the ^{10}Be method has been the dating of loess deposits in China, associated, e.g., with paleoprecipitations which originated about 500,000 years ago [66]. The ^{26}Al/^{10}Be burial dating of sedimentary infill combined with magnetic reversal stratigraphy has been used in paleoanthropology to demonstrate the presence of past hominins during the last million years [67]. Other applications included a searching for past earthquakes, important when building NPPs, with the idea to enlarge the ^{14}C time span (only up to 50 ky), when compared to ^{10}Be (a few million years) [68].

Extraterrestrial studies included analysis of ^{10}Be in meteorite and lunar samples with the aim of studying long-term variations of cosmic rays, to determine cosmic-ray exposure ages of meteorites, their pre-atmospheric dimensions and their terrestrial ages [69–71].

AMS measurements of ^{10}Be

To successfully quantify the presence of ^{10}Be in samples, the material must undergo a complex chemical treatment protocol [72] with the aim of extracting Be from the sample, removing B (^{10}B isobar is the primary source of background for ^{10}Be in AMS measurements), and transform the Be from the sample into a suitable form for AMS measurement (BeO being the most used chemical form). The extraction of Be is dependent on the specific sample matrix, but in general it is based on mechanical and chemical disruption of the sample matrix and subsequent leaching of Be. The separation of Be and its purification from leachate is usually done by ion exchange chromatography. The resulting beryllium hydroxide is then combusted to form beryllium oxide, which is a material suitable for use in AMS. The resulting oxide is mixed with Nb powder and pressed into cathodes used in ion sources. Since the AMS measurement of ^{10}Be is primarily limited by its isobar ^{10}B, even after a rigorous sample preparation protocol, ^{10}B is still present in the sample and its influence needs to be resolved during the AMS measurement itself. AMS systems use the higher energy loss of ^{10}B in matter compared to ^{10}Be, which is achieved by placing a gas or foil absorber in front of the detector or a degrader foil with subsequent magnetic/electrostatic separation [73, 74]. Ionization chambers with segmented anodes are routinely used as the end-of-the-line detectors to enable $\Delta E - E$ measurements to further suppress the ^{10}B background [75].

Preliminary AMS measurements of ^{10}Be carried out at the CENTA facility used instead of a large high-resolution magnet only a small switching magnet, SiN foil as an absorber for ^{10}B isobar suppression and an ionization chamber as the end-of-the-line detector [76]. The MC-SNICS ion source was used for the production of ^{10}BeO$^-$ ions, which were mass separated and injected into the 9SDH-2 Pelletron, operating at 3 MV terminal voltage. The ^{10}Be^{2+} ions were

selected to be analyzed (Fig. 4), and the ^{10}B ions, as well as most of the background ions from heavier ions, were absorbed in the silicon nitride stack introduced in front of the ionization chamber. An ionization chamber with two cathodes was used for the ion detection. In these measurements, the standard ^{10}Be source with the $^{10}Be/^{9}Be$ mass ratio of $(8.71 \pm 0.24) \cdot 10^{-11}$ was used. Using this setup, a detection limit for $^{10}Be/^{9}Be$ of the order of 10^{-12} was achieved, which was mainly determined by scattering of $^{9}Be^{2+}$ ions (energy of 7.059 MeV) in residual gas inside the switching magnet. This has been the first application of the switching magnet described in the literature for the successful analysis of ^{10}Be by the AMS technique. However, the detection limit obtained with the switching magnet is too high for most of environmental applications. Recent measurements conducted using the newly installed high-resolution magnet, two 45° electrostatic analyzers, and a multilayer ionization chamber (with four anodes, one cathode, a Frish grid and an entrance window for isobar elimination) improved the detection limit for the $^{10}Be/^{9}Be$ ratio to $7 \cdot 10^{-15}$.

Aluminum-26

Motivation

Cosmogenic ^{26}Al has been the most frequently used in astrophysics for investigations of lunar and meteorite samples. Similarly, as for ^{10}Be, the ^{26}Al is also produced in interactions of cosmic-ray particles with these extraterrestrial bodies. The determination of cosmic-ray exposure ages of meteorites and their pre-atmospheric sizes has been the main applications of ^{26}Al. Therefore, the ^{10}Be and ^{26}Al couple has been very useful in these investigations, as it allows much better sensitivity and precision compared with single applications of these cosmogenic radioisotopes [69]. The terrestrial production of ^{26}Al by cosmic rays in the atmosphere in nuclear reactions with argon (meteoric ^{26}Al), as well as in nuclear reactions with silicon present in minerals (in situ production) is much lower when compared with ^{10}Be, therefore, the abundance of ^{26}Al in the terrestrial environment is considerably lower than ^{10}Be. Analysis of meteoric ^{26}Al is relatively rare due to its low abundance in environmental samples. However, new research indicates that the measurement of meteoric ^{26}Al in tandem with meteoric ^{10}Be is a promising chronometer for very old ice [77]. In situ ^{26}Al in terrestrial samples is used in the same way as ^{10}Be, mainly for surface exposure dating and burial dating. The ^{26}Al is especially important for sediment burial dating, because this method requires measurement of two different cosmogenic radionuclides produced in situ, and $^{26}Al/^{10}Be$ burial dating is one of its most used methods [67, 78]. It has also been used successfully for studies of the evolution of seismically active fault zones [68].

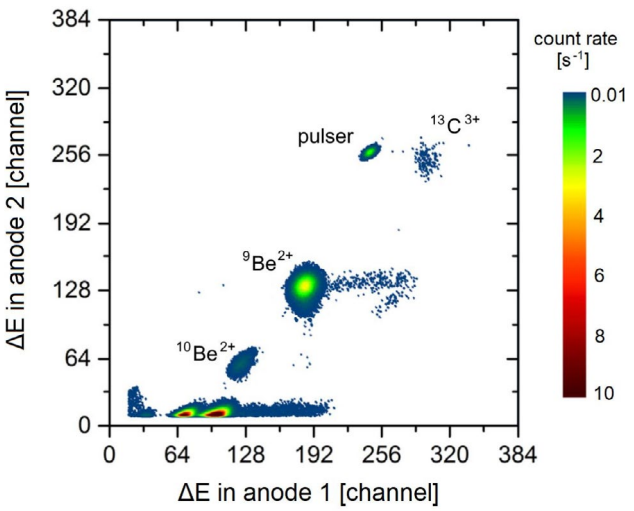

Fig. 4 Multidimensional mass spectra of Be ions measured in the ionization chamber with two cathodes and a silicon nitride stack absorber. The ^{10}B isobar was not observed, because the thickness of the Si_3N_4 foil stack was optimized for its complete energy deposition

AMS measurements of ^{26}Al

As ^{26}Al and ^{10}Be have similar chemical behavior, sample preparation procedures are almost identical [72]. The mechanical/chemical pretreatment and leaching steps are identical to ^{10}Be, the only difference is in the last steps of the ion exchange chromatography, where Al is eluted. The resulting aluminum hydroxide is then combusted to form aluminum oxide. The Al_2O_3 is mixed with Ag powder and the mixture is pressed into cathodes for use in the AMS ion source. In terms of AMS measurements, the important isobar of ^{26}Al is ^{26}Mg, but it does not form stable negative ions. The limiting factor in the AMS analysis of ^{26}Al is the relatively low Al^- ion current produced from Al_2O_3. AlO^- ion yields are several times higher, but MgO^- ions are stable and represent a significant background for AMS measurement of ^{26}Al, requiring an additional isobar suppression [79, 80].

Therefore, we have been looking for alternatives to Al_2O_3 that could be used in AMS measurements [81]. A comparison of the optimized negative ion beam currents obtained at CENTA (Table 2) shows that the best choice of aluminum material for AMS measurements are aluminum oxide and aluminum nitride, as these compounds provide sufficient electrical current for Al^-, AlN^- and AlO^- injected ions. On the other hand, aluminum sulphate and aluminum fluoride are not suitable materials for ^{26}Al measurements due their very low sputtering efficiency.

The Al_2O_3, AlN, pure aluminum wire and Mg_3N_2 were tested for $^{24-26}Mg^{14}N^-$ isobaric molecular interferences

by the formation of $^{26}Mg^{14}N^-$, which is the main isobaric interference for $^{26}Al^{14}N^-$. Mass scans of materials carried out at the high-energy part of the accelerator system (for the injected mass of ions of 41 amu) did not show any isobaric interferences (Fig. 5). However, AMS measurements with the same Al_2O_3, AlN and Mg_3N_2 matrices carried out in the VERA laboratory using 3 MV Pelletron with ^{26}Al-free blanks, showed that for ^{26}Al using AlN^- as the injected ion, further isobar suppression would be needed due to the high $^{26}Mg^{3+}$ production rate. This could be achieved either by a reaction cell, a gas filled magnet, or with an ion-laser interaction system. Therefore, aluminum oxide will probably remain the most frequently used in the analysis of ^{26}Al by AMS.

New AMS line in the CENTA laboratory

The presented results show that it is important to continue monitoring ^{14}C levels in the atmosphere and biosphere at urban sites, in clean air locations, and areas in the vicinity of NPPs. AMS has been a very helpful tool for such investigations, not only because it allows for a higher sample throughput, but also because it enables one to reach a better precision and accuracy of results with very small samples. This is important for the new generation of very fine $\Delta^{14}C$ studies in the atmosphere and biosphere with almost zero contributions from atmospheric nuclear weapons tests and the predominance of the Suess effect. Another important application includes climate change studies (e.g., impact of the Sun on Earth), where high precision ^{14}C measurements with target uncertainty of 1‰ will play an important role. AMS represents therefore a revolutionary development in the analytics, as it is the most sensitive technology for isotope analysis, achieving excellent detection limits and reducing the required sample size (e.g., for ^{14}C analysis down to micrograms of carbon).

Recently, a fully equipped beam line for AMS measurements was installed at the CENTA, with the aim to combine new ion beam technologies—Ion Beam Analysis (IBA) and AMS, and their wide-range applications. The CENTA has been running a tandem laboratory for ion beam analysis (IBA) equipped with MC-SNICS and Alphatross ion sources, the injection beam line, the Pelletron tandem accelerator with 3 MV terminal voltage, and the post-acceleration beam lines [32, 82, 83], mostly used for IBA analyses.

The newly installed AMS units included (Fig. 6):

- Bouncing system in the injection beam line with a multi-Faraday cup for acceptance of ^{9}Be, ^{12}C and ^{13}C ions, plus the second one for ^{27}Al and other isotopes,

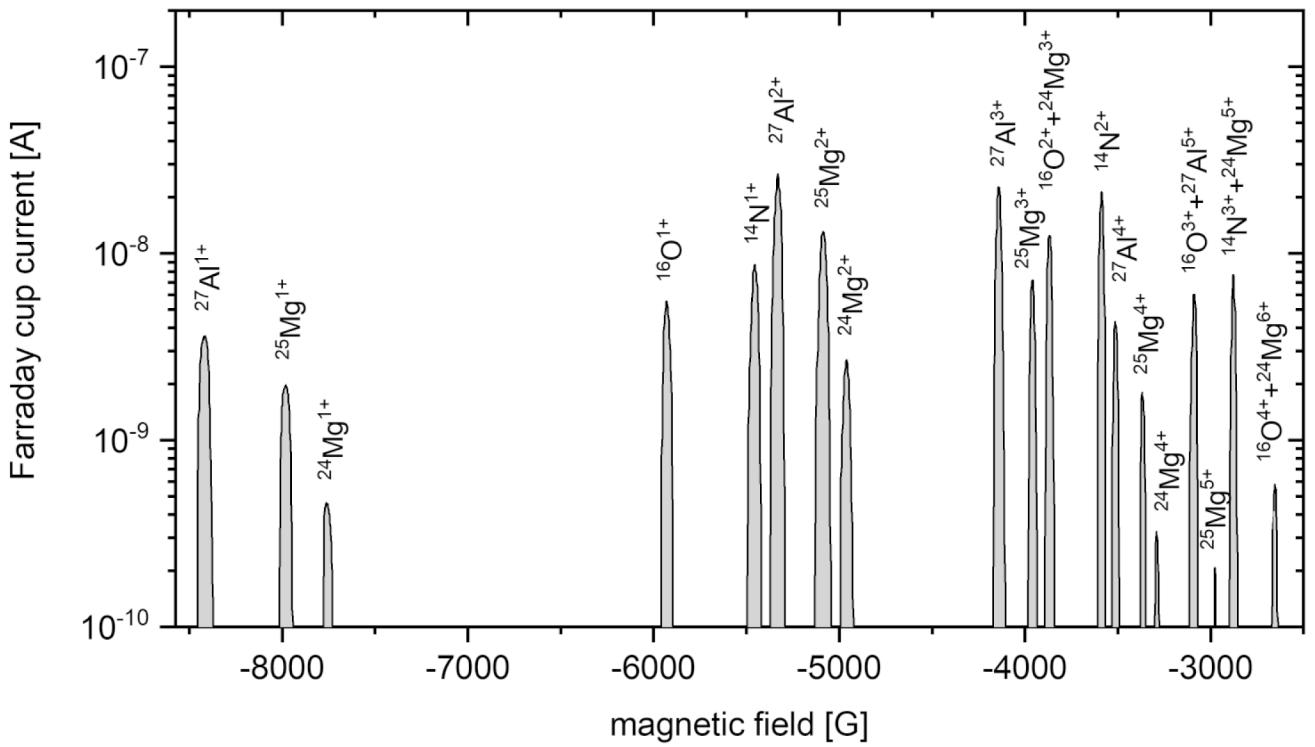

Fig. 5 Mass scans of ions from the Mg3N2 sample after acceleration and dissociation. Injected mass of ions was 41 amu (possibly a combination with $\{[^{24-26}Mg$ or $^{27}Al][^{14}N$ or $^{16}O][H0\text{-}3]\}^-$)

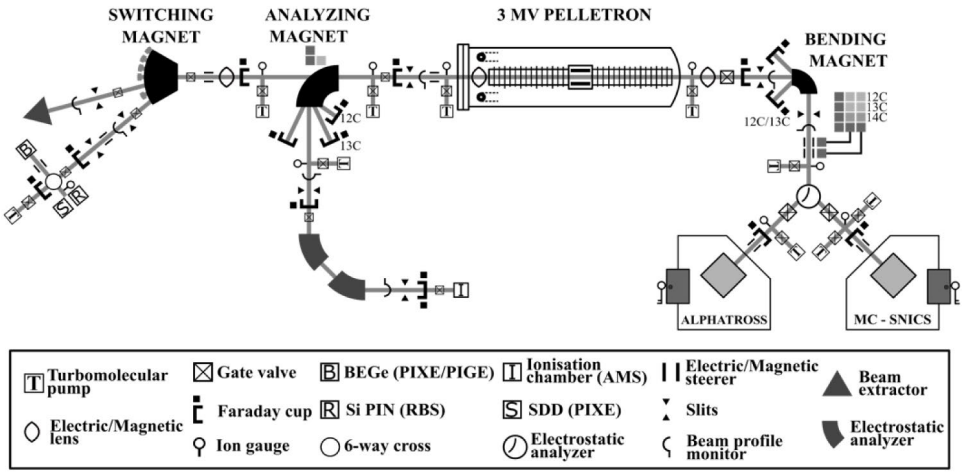

Fig. 6 AMS beam line installed the in the CENTA laboratory: a floor scheme (top), installed units (middle), and a detail of the end-of-the-line ionization chamber detector (bottom)

Fig. 7 Two-dimensional ^{14}C spectrum of the NIST oxalic acid standard (OXA II) (top) and corresponding background (bottom) measured by the end-of-the line ionization chamber

- Electrostatic quadrupole for ion focusing (installed inside the Pelletron accelerator),
- High-resolution electromagnet ($ME/Z^2 = 176$ amu-MeV),
- Multi-Faraday chamber with three Faraday cups for the detection of ^{9}Be, ^{12}C, ^{13}C, ^{127}I ions and other ions),
- Two 45° electrostatic analyzers,
- End-of-the-line detector (a multilayer ionization chamber with 4 anodes, one cathode, a Frish grid, and an entrance window for isobar elimination.

Performance tests of the AMS system have been carried out for several long-lived radionuclides, including ^{14}C standards and background targets. A fast-bouncing system for sequential injection of $^{12}C^-$, $^{13}C^-$ and $^{14}C^-$ was used. The terminal voltage of the tandem accelerator was maintained at 2.7 MV. The stripping yield of the 3^+ ions was 40–45%. The $^{12}C^{3+}$ ions as reference ions were measured in the off-side Faraday cup. The detector window of the ionization chamber with 5 µm Mylar foil was used for the registration of $^{14}C^{3+}$ions. The two-dimensional ^{14}C spectra of the NIST (National Institute of Standards and Technology, Gaithersburg, USA) oxalic acid standard reference material SRF-4990C (OXA II) and the background measured by the multilayer ionization chamber are presented in Fig. 7. The measured average $^{14}C/^{12}C$ ratio of the OXA II standard was $1.162 \cdot 10^{-12}$, and the background of the synthetic graphite sample (Alfa Aesar) was $2 \cdot 10^{-15}$, in good agreement with measurements in other AMS laboratories [84]. The measured scatter of the OXA II ^{14}C standard data

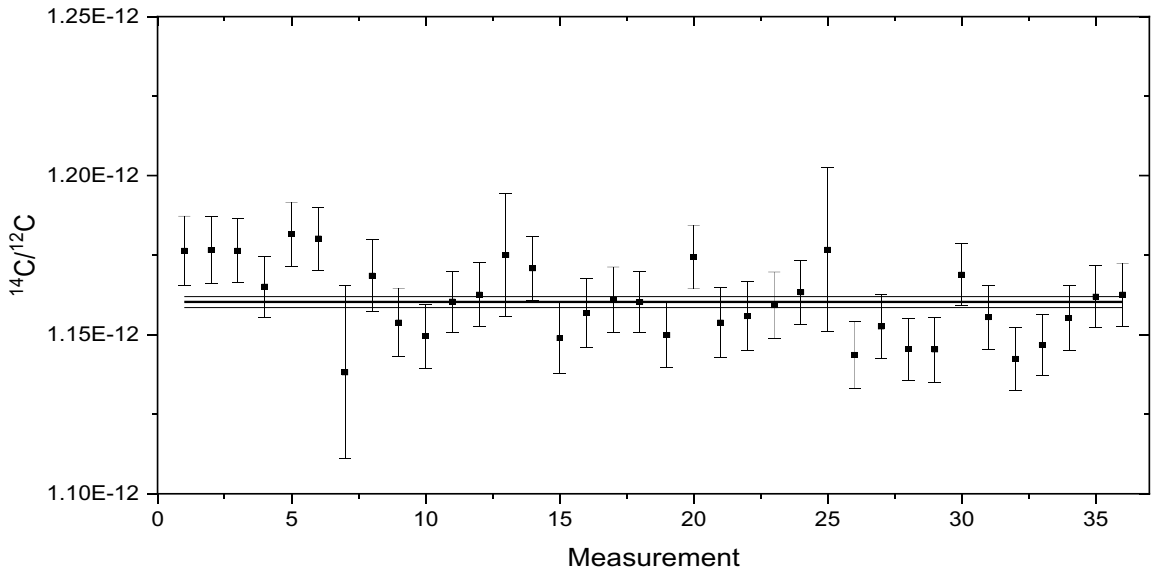

Fig. 8 Measured scatter of the NIST OXA II ^{14}C standard data (a weighted mean of standard deviation (1.5 ‰) is also shown)

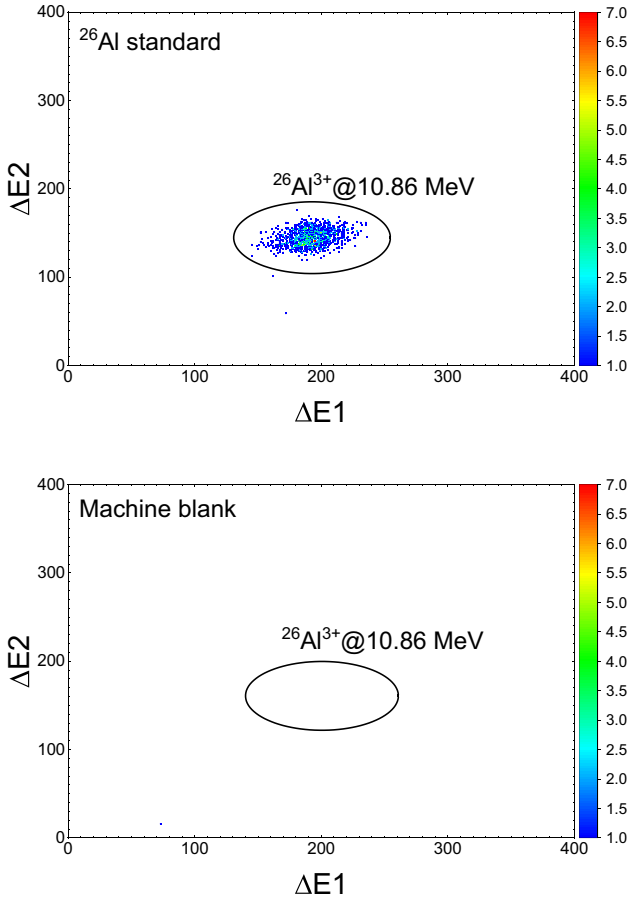

Fig. 9 Two-dimensional ^{26}Al spectrum of the standard (top) and corresponding background (bottom) measured by the end-of-the-line ionization chamber (counting rate s^{-1})

showed a weighted mean of standard deviation of 1.5 ‰ (Fig. 8).

In the case of ^{26}Al analyzes, a fast-bouncing system was used for sequential injection of $^{26}Al^{-}$ and $^{27}Al^{-}$. The terminal voltage of the tandem accelerator was maintained at 2.7 MV. The stripping yield of the 3^{+} ions was 35–40%. The $^{27}Al^{3+}$ ions as reference ions were measured in the off-side Faraday cup. The detector window of the ionization chamber with 100 nm Si_3N_4 foil was used to register $^{26}Al^{3+}$ ions. The $^{26}Al/^{27}Al$ machine background was $5{\cdot}10^{-15}$. The two-dimensional spectra of the ^{26}Al standard and the background are shown in Fig. 9.

Conclusions

The AMS has become the most sensitive technique for ultralow-level analyses of long-lived radioisotopes [85], specifically for ^{14}C analyses in tree rings, and ^{10}Be and ^{26}Al in terrestrial and extraterrestrial archives (e.g., in geological samples and meteorites). However, ICPMS also did recently a great progress, e.g., in analysis of ^{135}Cs and ^{137}Cs radioisotopes in seawater [86].

We discussed recent developments in AMS methods for ^{14}C, ^{10}Be and ^{26}Al measurements with emphasis on applications carried out at the Centre for Nuclear and Accelerator Technologies (CENTA). The AMS technology in the CENTA will be applied to several branches of basic and applied research, including nuclear sciences, astrophysics, environmental sciences, climate change studies, material research, biomedical sciences, forensics, etc. Together with existing low-background gamma-spectrometry laboratory [87], the CENTA will represent a unique laboratory for radioactivity research.

Acknowledgements The authors acknowledge the support provided by the Operational Program Integrated Infrastructure for the project "Advancing University Capacity and Competence in Research, Development and Innovation (ACCORD)", (ITMS2014+:313021X329), co-financed by the European Regional Development Fund. The support from the Slovak Research and Development Agency (projects APVV-15-0576 and APVV-21-0377) and from the Slovak Science Grant Agency (projects VEGA-1/0625/21 and VEGA-1/0487/23) are also acknowledged.

Data availability The datasets analyzed and/or used in the current study are available from the corresponding author (Pavel Povinec) and can be provided on a reasonable request at pavel.povinec@uniba.sk.

Declarations

Conflict of interest The authors declare that they have no known competing financial interests or personal relationships.

References

1. Povinec PP et al (2008) Acta Phys Slov 58:1–154
2. Povinec PP (2017) Appl Radiat Isot 126:26–30
3. Laubenstein M (2017) Int J Mod Phys A 32:1743002
4. LaFerriere BD et al (2015) Nucl Instrum Meth Phys Res A 775:93–98
5. Nisi S et al (2009) Appl Radiat Isot 67:828–832
6. Famulok N et al (2015) Nucl Instrum Meth Phys Res B 361:193–196
7. Walner A et al (2016) Nature 532:69–72
8. Reimer P et al (2020) Radiocarbon 62:725–757
9. Petit JR et al (1999) Nature 399:429–435

10. Kanzava K et al (2021) J Geophys Res Space Phys 126:e2021JA029378
11. Stuiver M (1965) Science 149:533–535
12. Burchuladze AA et al (1980) Nature 287:320–322
13. Miyake F et al (2012) Nature 486:240–242
14. Jull AJT et al (2018) Radiocarbon 60:1237–1248
15. Brehm N et al (2021) Nature Geosci 14:10–15
16. Nydal R, Lövseth K (1965) Nature 206:1029–1031
17. Burchuladze AA et al (1989) Radiocarbon 31:771–776
18. Livingston HD, Povinec PP (2002) Health Phys 82:656–668
19. Povinec PP, Hirose K, Aoyama M (2013) Fukushima accident: radioactivity impact on the environment. Elsevier, New York, p 385p
20. Povinec PP et al (2013) Biogeosciences 10:5481–5496
21. Kaizer J, Nisi S, Povinec PP (2019) J Radioanal Nuc Chem 322:1447–1454
22. Povinec PP (2013) J Radioanal Nucl Chem 295:537–544
23. Levin I et al (2022) Radiocarbon 64:781–791
24. Keeling CD (1979) Environ Intern 2:229–300
25. Broecker WS (1991) Oceanography 4:79–89
26. Povinec P et al (1968) Intern J Appl Radiat Isot 19:877–881
27. Povinec P (1972) Radiochem Radioanal Lett 9:127–135
28. Povinec P (1978) Nucl Instrum Meth 156:441–445
29. Levin I et al (1985) Radiocarbon 27:1–19
30. Turnbull JC et al (2017) Atmosph Chem Phys 17:14771–14784
31. Ješkovský M et al (2015) Nucl Instrum Meth Phys Res B 361:129–132
32. Povinec PP et al (2015) Nucl Instrum Meth Phys Res B 361:87–94
33. Kontul' I et al (2017) Appl Radiat Isot 126:58–60
34. Kontul' I et al (2020) J Environ Radioact 218:106237
35. Kontuľ I et al (2022) Radiocarbon 64:1577–1585
36. Hammer S, Levin I (2017) Monthly mean atmospheric $\Delta^{14}CO_2$ at Jungfraujoch and Schauinsland from 1986 to 2016. https://doi.org/10.11588/data/10100, heiDATA, V2
37. Stuiver M, Polach HA (1977) Radiocarbon 19:355–363
38. Kuc T et al (2007) Radiocarbon 49:807–816
39. Rakowski AZ et al (2004) Radiocarbon 46:911–916
40. Rakowski AZ, Nakamura T, Pazdur A (2008) J Environ Radioact 99:1558–1565
41. Rakowski AZ et al (2013) Nucl Instrum Meth Phys Res B 294:503–507
42. Svetlik I et al (2010) Radiocarbon 52:823–834
43. Svetlik I et al (2012) J Radioanal Nucl Chem 291:689–695
44. Li Y et al (2016) Sci Total Environ 539:515–525
45. Ramanathan V, Carmichael G (2008) Nature Geosci 1:221–227
46. Contini D, Vecchi R, Viana M (2018) Atmosphere 9:181
47. Szidat S et al (2006) Atmos Chem Phys 9:1521–1535
48. Major I et al (2015) Radiocarbon 57:991–1002
49. Dusek U et al (2017) Atmos Chem Phys 17:3233–3251
50. Santos GM et al (2007) Nucl Instrum Methods Phys Res B 259:293–302
51. Genberg J et al (2010) Atmos Chem Phys 11:11387–11400
52. Povinec P et al (1988) J Radioanal Nucl Chem Lett 126:467–478
53. Povinec PP et al (2012) J Environ Radioact 108:33–40
54. Sýkora I et al (2017) J Environ Radioact 166:27–35
55. Sýkora I, Povinec PP (2020) J Radioanal Nucl Chem 325:245–252
56. Povinec PP et al (2012) J Environ Radioact 114:81–88
57. Povinec PP, Hirose K, Aoyama M, Tateda Y (2021) Fukushima Accident: 10 years after. Elsevier, New York, p 560p
58. Kontuľ I et al (2020) J Environ Radioact 218:106221
59. Beer J et al (1990) Nature 347:164–166
60. Zhou et al (2010) Radiocarbon 52:129–136
61. Balco G (2011) Quat Sci Rev 30:3–27
62. Zhang et al (2016) Radiocarbon 58:193–203
63. Matmon A et al (2012) Bull Geol Soc Am 124:626–640
64. Kučera J et al (2023) Chem Listy 117:107–113
65. Jelinski NA et al (2019) J Geophys Res Earth Surf 124:874–901
66. Beck JW et al (2018) Science 360:877–881
67. Carbonell E et al (2008) Nature 452:465–469
68. Šujan M (2019) Sediment Geol 383:248–267
69. Eugster O (2003) Chem Erde 63:3–30
70. Jull, (2006) Terrestrial ages of meteorites. In: Lauretta D, McSween HY (eds) Meteorites and the early Solar System II. The University of Arizona Press, Tucson, pp 889–905
71. Jull AJT (2013) Radiocarbon 55:1779–1789
72. Merchel S et al (2019) Nucl Instr Meth Phys Res B 455:293–299
73. Klein MG et al (2008) Nucl Instr Meth Phys Res B 266:1828–1832
74. Kumar P et al (2011) J Radioanal Nucl Chem 290:179–182
75. Fifield LK et al (1990) Nucl Instr Meth Phys Res B 52:233–237
76. Ješkovský M et al (2015) Nucl Instr Meth Phys Res B 361:139–142
77. Auer M et al (2009) Earth Planet Sci Lett 287:453–462
78. Granger DE, Muzikar PF (2001) Earth Planet Sci Lett 188:269–281
79. Kislinger G et al (1997) Nucl Instr Meth Phys Res B 123:259–265
80. Arazi A et al (2004) Nucl Instr Meth Phys Res B 223–224:259–262
81. Pánik J et al (2019) Nucl Instr Meth Phys Res B 438:101–106
82. Povinec PP et al (2015) Nucl Instr Meth Phys Res B 342:321–326
83. Povinec PP et al (2016) J Radioanal Nucl Chem 307:2101–2108
84. Kučera J et al (2023). Chem Papers. https://doi.org/10.1007/s11696-023-02904-2
85. García-León M (2022) Detecting environmental radioactivity. Springer Nature, Cham
86. Zhu L, Hou X, Qiao J (2021) Talanta 226:122121
87. Povinec PP et al (2009) J Radioanal Nucl Chem 282:805–808